Biosensors and Bioelectronics 85 (2016) 883–890

Contents lists available at ScienceDirect

Biosensors and Bioelectronics

journal homepage: www.elsevier.com/locate/bios

# An amperometric nanobiosensor using a biocompatible conjugate for early detection of metastatic cancer cells in biological fluid

Ramjee Pallela [a,1], Pranjal Chandra [b,*,1], Hui-Bog Noh [a], Yoon-Bo Shim [a,*]

[a] Department of Chemistry and Institute of BioPhysio Sensor Technology (IBST), Pusan National University, Busan 609–735, South Korea
[b] Department of Biosciences and Bioengineering, Indian Institute of Technology Guwahati, Guwahati 781039, Assam, India

ARTICLE INFO

*Article history:*
Received 8 April 2016
Received in revised form
20 May 2016
Accepted 30 May 2016
Available online 31 May 2016

*Keywords:*
Cancer metastasis
Cancer cells
Nanobiosensor
Electrochemistry
Conducting polymer
Early diagnosis

ABSTRACT

Metastasis is the major cause of cancer-associated death in humans, and its early diagnosis will help clinicians to develop suitable therapeutic strategies which may save life of cancer patients. In this direction, we designed an amperometric biosensor using a biocompatible conjugate to diagnose cancer metastasis by detecting epithelial cell adhesion molecule expressing metastatic cancer cells (Ep-MCCs). The sensor probe is fabricated by immobilizing monoclonal capture antibody (CapAnti) on the gold nanoparticles (AuNPs)/conducting polymer composite layer. The detection relies on a sandwich-type approach using a bioconjugate composed of reporter antibody (RepAnti), nanostructured collagen (nCOL), AuNPs, and hydrazine (Hyd) which served as a nonenzymatic electrocatalyst for the reduction of $H_2O_2$. The binding of Ep-MCCs with the sensor probe was confirmed using electrochemical impedance spectroscopy, cyclic voltammetry, and chronoamperometry. A dynamic range for the Ep-MCCs detection is determined between 45 and 100,000 Ep-MCCs/mL with the detection limit of $28 \pm 3$ Ep-MCCs/mL. The proposed immunosensor is successfully applied to detect Ep-MCCs in serum and mixed cell samples and interferences due to nontarget cells and molecules present in the real sample matrix are also examined. The early stage of Ep-MCCs was examined by fluorescence-activated cell sorting assay, which confirms that the developed biosensor has detected Ep-MCCs in its early stage.



## 1. Introduction

Among all the life threatening diseases, cancer is one of the most common cause of death worldwide and can exist in two hundred diverse forms including lung, neuroblastoma, pancreas, breast, bone, ovarian, gastrointestinal, colon, bladder, *etc.* (Pecorino, 2012). Cancer associated mortality occurs mainly due to cancer metastasis, a condition in which cancer cells migrates form one position to another and forms secondary tumors (Chambers et al., 2002). Therefore, it is extremely essential and clinically significant to diagnose cancer metastasis at its early stage to save or prolong the life of cancer patients. In medical science, a metastatic condition is confirmed due to the presence of special type of cancer cells, called as metastatic cancer cells (MCCs), which later on forms secondary tumors (Camacho, 2012; Krebs et al., 2010). Thus, detecting MCCs would be very helpful to diagnose cancer metastasis. Liquid biopsy is preferred to diagnose cancer metastasis through detecting MCCs or cell-free circulating tumor DNA (Karachaliou et al., 2015). Biomarker based-cancer cell detection is effective (de la Escosura et al., 2009) and provides valuable information that is helpful for oncologist to design adequate therapeutic strategies. To detect MCCs, epithelial cell adhesion molecule (EpCAM), a transmembrane glycoprotein antigen has been targeted enormously which is expressed on MCC surface in abundance (Nagrath et al., 2007) and absent on blood cells (Panchapakesan et al., 2010). Thus, the EpCAM expressing MCCs (Ep-MCCs) is considered as clinically relevant biomarker to diagnose cancer metastasis. Various techniques, such as; immunohistochemistry (Spizzo et al., 2011), fluorescent *in situ* hybridization (Katz et al., 2010), reverse transcription polymerase chain reaction (Zhao et al., 2013), immunomagnetic assay (Königsberg et al., 2011), reflectometric interference spectroscopy (Kumeria et al., 2012), flow cytometry (Skirecki et al., 2014) have been applied to detect Ep-MCCs. These methods are valuable, however, they have limited point-of-care clinical applications because they are multistep, require highly trained professionals, and the lack of miniaturization ability for onsite analysis. Few biosensor-based methods have also been reported to detect Ep-MCCs (Arya et al., 2013; Moscovici et al., 2013), but they are less sensitive, possess narrow detection range, and require advance microfabrication techniques. Additionally, the reported methods are not integrated with Ep-MCCs physiological

* Corresponding authors.
*E-mail addresses:* pchandra13@iitg.ernet.in (P. Chandra), ybshim@pusan.ac.kr (Y.-B. Shim).
[1] Equal contribution

http://dx.doi.org/10.1016/j.bios.2016.05.092
0956-5663/

stage characterization before cytosensing, which is the most important criteria to demonstrate early diagnosis of cancer metastasis. Thus, the development of a sensitive, robust, and alternate method for the detection of Ep-MCCs in biological fluids is valuable and to diagnose cancer metastasis. To achieve a highly sensitive detection of Ep-MCCs, an electrochemical sensor combined with non-enzymatic catalytic reporter probe is worthy to attempt due to their high selectivity, stability, and sensitivity. The stable immobilization of antibodies on the sensor probe surface is very important in the biosensor fabrication (Rahman et al., 2008). Electrochemical biosensors fabricated using conducting polymers-AuNPs composite are considered to be highly stable and ultrasensitive because biomolecules can be covalently immobilized on the polymer backbone possessing –COOH or $–NH_2$ groups (Chandra et al., 2012; Rahman et al., 2008). Usually, nanomaterials, such as metal nanoparticles, carbon nanotube, graphene are used to prepared cytosensors, but they cannot be always used due to their cellular toxicity (Feng and Liu, 2011; Zhang et al., 2010). Therefore, biosensor fabrication using biocompatible nanostructures is important for cytosensing applications. One of the promising biomaterial is collagen, which acts as an adherent cytocompatible material, probe material, and has been used to prepare collagen nanoparticles or nanostructured collagens (nCOL) (Nicklas et al., 2009). Therefore, it is worthy to attempt collagen nanoparticles as an alternate detection probe matrix other than graphene or CNT to detect cancer cells.

To obtain signal in an electrochemical immunosensor, a redox-indicator molecule such as a bioconjugate composed of enzyme or nonenzymatic catalyst is required (Chandra et al., 2015). Of these, the use of AuNPs has been proven to be a reliable (Hermanson, 2013), but the stability of the system is open for debate. Therefore, we have prepared a semiconducting nanostructured collagen as a binding material, since the material is highly bio-compatible and shows no cytotoxicity (Anderson and Eriksson, 1968; Mukherjee et al., 2011). It forms a stable composite with AuNPs to enhance the signal and provides a suitable substrate for the immobilization of the secondary antibody. Therefore, this system can be further applied to develop biocompatable *in vitro* nanobiosensors. In addition, a chemical electrocatalyst, hydrazine (Hyd) attached on a bioconjugate is of great interest compared to costly and easily denatured enzymes due to its small size, stability, and high catalytic activity towards hydrogen peroxide ($H_2O_2$) reduction (Zhu et al., 2013). Thus, a sandwich type nanobiosensor having chemo-nano-bio-conjugate composed of Hyd, nCOL, AuNPs, and RepAnti has been applied to detect Ep-MCCs.

In the present study, a nonenzymatic sandwich type biocompatable amperometric nanobiosensor has been developed to detect metastatic cancer cells directly in biological matrix for the first time. The nanobiosensor was characterized by X-ray photoelectron spectroscopy (XPS), electrochemical impedance spectroscopy (EIS), scanning electron microscopy (SEM), and quartz crystal microbalance (QCM). The experimental parameters were optimized and the detection limit of Ep-MCCs was determined. Direct detection of Ep-MCCs in serum and mixed cell samples were performed to evaluate the real clinical value of the developed sensor. The selectivity of the biosensor was also examined toward various non-target cells and chemicals present in the real sample matrix. Biocompatibility of the sensor was examined and fluorescence-activated cell sorting (FACS) was performed to examine the cell stage.

## 2. Experimental

### 2.1. Materials and instruments

2,2′:5′,2″-Terthiophene-3′(p-benzoic acid (TTBA)) was prepared using the Paal-Knorr pyrrole condensation reaction (Koh et al., 2011). Tetrabutylammonium perchlorate (TBAP, electrochemical grade) was purchased from Fluka (USA) and purified according to a general method, followed by drying under vacuum at $1.33 \times 10^{-3}$ Pa (Chandra et al., 2011a). Type I collagen (bovine), hydrazine sulfate, 1-Ethyl-3-(3-dimethylamino-propyl) carbodiimide (EDC), *N*-hydroxysuccinimide (NHS), gold(III) chloride trihydrate ($HAuCl_4 \cdot 3H_2O$), dichloromethane (99.8%, anhydrous, and sealed under $N_2$ gas), sodium citrate, sodium borohydrate ($NaBH_4$), EpCAM antibody, and $H_2O_2$ were purchased from Sigma-Aldrich (USA). Phosphate buffer was prepared using standard method. Human breast adenocarcinoma (SK-BR3 and MCF-7), human cervical carcinoma (HeLa), and human embryonic kidney carcinoma (HEK-293), jurkat cell lines were obtained from American Type Culture Collection. Dulbecco's Modified Eagle's Medium (DMEM) was purchased from BioWhittaker®, whereas RPMI-1640 medium, fetal bovine serum (FBS) and other cell culture materials including Dulbecco's PBS were purchased from Sigma-Aldrich (USA). The electrochemical measurements were performed using a three electrode electrochemical cell. The modified glassy carbon electrode (GCE) (dia. 3.0 mm), Ag/AgCl (in saturated KCl), and a platinum (Pt) wire were used as working, reference, and counter electrodes, respectively (Please see Supplementary material for details).

### 2.2. Preparation of bioconjugate

Nanostructured collagen (nCol) was prepared using bovine type I collagen by the alkaline hydrolysis following an earlier reported method (Nicklas et al., 2009). Briefly, the hydrolysis of collagen samples was carried out in 1.5 M NaOH under constant stirring (500 rpm) at room temperature for 56 h. Thereafter, the hydrolyzed sample was dialyzed (Sigma-Aldrich, 10–12 kDa cut-off) against deionized water and filtered through disposable syringe filter (DISMIC®-$25_{AS}$; Advantec, Tokyo, Japan). The freshly prepared nCol sample was mixed with 1.0 wt% $HAuCl_4$ and 1.0 mg/mL hydrazine sulfate solution and subjected to sonication for 30 min to get a homogenous suspension. To this solution, 400 μL RepAnti (optimized 80 μg/mL) was added and the whole mixture was incubated in a refrigerator overnight at 4 °C with mild stirring in dark following a previously reported method (Zhu et al., 2010). Then, the reaction mixture was centrifuged and the resulting deposit was washed five times with PBS (pH 7.4). Finally, the prepared RepAnti-nCOL-Hyd-AuNPs conjugate was stored at 4 °C for further use.

### 2.3. Biocompatibility analysis of bioconjugate using cytotoxicity assay

The cytotoxicity of bioconjugate was assessed using MTT [3-(4,5-dimethylthiazol-2-yl)-2,5-diphenyltetrazolium bromide] assay which depends on the transformation of a tetrazolium compound (MTT) to purple colored formazan crystals due to the activity of mitochondrial dehydrogenase present in cells (Srivastava et al., 2015). Detail procedure is described in Supplementary material.

### 2.4. Fabrication of immunosensor detection probe

The schematic of the immunosensor preparation is shown in Scheme 1. A layer of the polymer of the TTBA monomer was

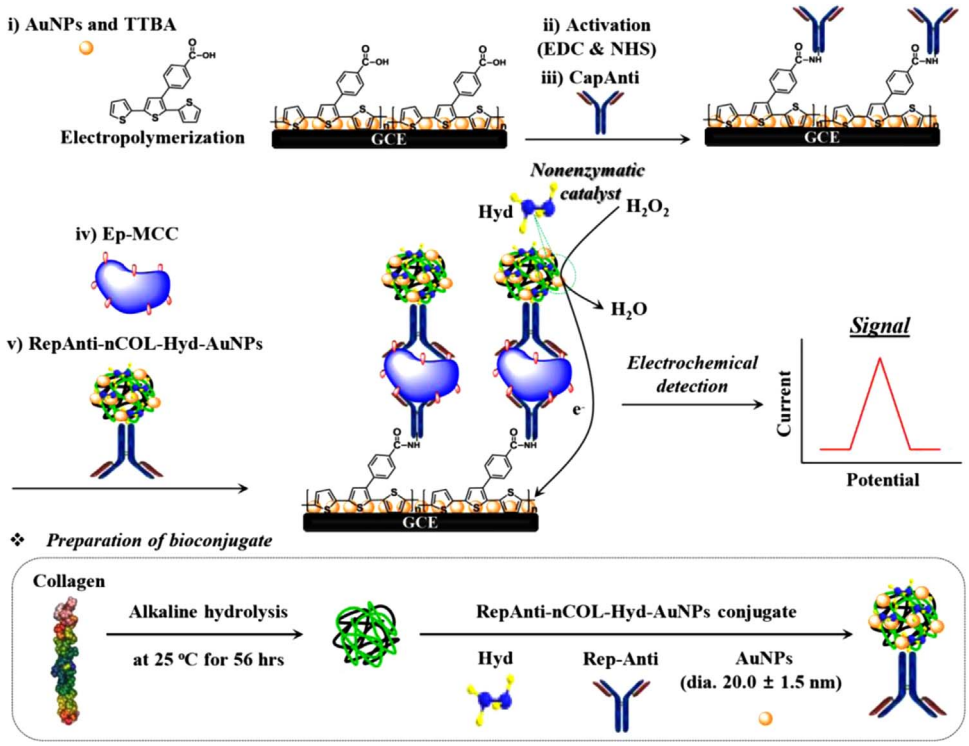


**Scheme 1.** Schematic representation of the immunosensor construction and detection principle.

formed on the GCE/AuNPs surface through electrochemical polymerization of 1.0 mM solution of the TTBA monomer in a 0.1 M TBAP/$CH_2Cl_2$ by a single potential cycling from 0.0 to +1.4 V at a scan rate of 100.0 mV $s^{-1}$. This was followed by activation of –COOH groups using EDC/NHS of pTTBA, followed by immobilization of CapAnti on the nanocomposite film (Please see Supplementary material for details).

### 2.5. Cancer cells sample preparation, FACS analysis, and detection of Ep-MCCs with the sensor probe

The cells were cultured in 75 $cm^2$ tissue culture flask at 37 °C in 5% $CO_2$ atmosphere in the appropriate medium supplemented with a 10% heat-inactivated FBS, 100 units/mL of penicillin and streptomycin. The medium was replaced every two days while running the experiments. Before each experiment, cells were suspended in autoclaved PBS and counted using a disposable C-Chip (South Korea).

Before detecting Ep-MCCs using the nanobiosensor, the cell cycle analysis by FACS was performed to know the stage of Ep-MCCs. Briefly, $1 \times 10^6$ Ep-MCCs were fixed in 0.7 mL of 70% ethanol for 16 h and then centrifuged at 2000 rpm for 10 min and washed with autoclaved PBS. The Ep-MCCs were re-suspended in 40 μL of PBS and treated with 10 μL RNase (20 μg/mL prepared in PBS) and were incubated at 37 °C for 60 min in a heat block. Next, 20 μL propidium iodide stain (250 μg/mL) was added and the sample was incubated at 4 °C for 20 min. Finally, the Ep-MCC sample was transferred into the FACS tube (Falcon™ 5 mL) and analyzed using the BD FACS Calibur flow cytometer (BD Biosciences, USA). The results were shown in terms of the relative cellular DNA content in the cells at different cell stages. In the next step, the prepared Ep-MCCs were detected using the nanobiosensor as shown in Scheme 1. The details of Ep-MCCs detection using the nanobiosensor is described in the Supplementary material.

## 3. Results and discussion

### 3.1. Characterization and morphology of sensor probe

At first, the AuNPs were electrodeposited onto the GCE using LSV where the reduction peak currents increased with increase in the number of sweeps which clearly shows the successful deposition of AuNPs (figure not shown). The results obtained for the AuNPs electrodeposition were comparable with our previously reported results (Chandra et al., 2011b). Next, the pTTBA film was formed on the GCE/AuNPs surface by electropolymerization from a 1.0 mM TTBA monomer solution. The monomer oxidation peak was obtained at +1.2 V during the anodic scan between 0.0 and +1.4 V and a clear reduction peak at +0.8 V in the reverse cathodic scan was observed which corresponds to the reduction of the oxidized polymer film formed on the GCE/AuNPs surface. The results related to nanocomposite film fabrication were in agreement with our earlier reported result (Noh et al., 2012). Each modification steps were characterized using XPS, QCM, SEM, TEM, and AFM in detail. At first, we characterized the biosensor using XPS, taken after 50s of Ar ion gas etching and calibrated with a C1s peak at 284.6 eV as an internal standard. Fig. 1(A) shows the deconvoluted XPS spectra of the (a) Au4f, (b) C1s, (c) S2p, and (d) N1s. After the electrodeposition of AuNPs onto the GCE, two sharp peaks appeared at 87.2 and 83.6 eV that correspond to Au4f (Fig. 1(A(a))), indicating the successful AuNPs deposition. The intensities of the Au4f peaks, however, decreased after polymerization on TTBA showing coating of pTTBA onto the GCE/AuNPs. The C1s spectrum for pTTBA surface shows two distinct peaks at 283.3 and 284.0 eV that are related to the C=C, C–C, C–H, or C–S bonds, and a C=O, C–O bonds, respectively (Fig. 1(A(b(i)))). After immobilization of the CapAnti (GCE/AuNPs/pTTBA/CapAnti), a new peak corresponding to C–N bond appeared at 284.1 eV due to the bond formation between –COOH groups of pTTBA and $–NH_2$ groups of CapAnti, the peak due to C=O bond was shifted toward the high energy at 285.1 eV (Fig. 1(A(b(ii)))). The pTTBA coated film

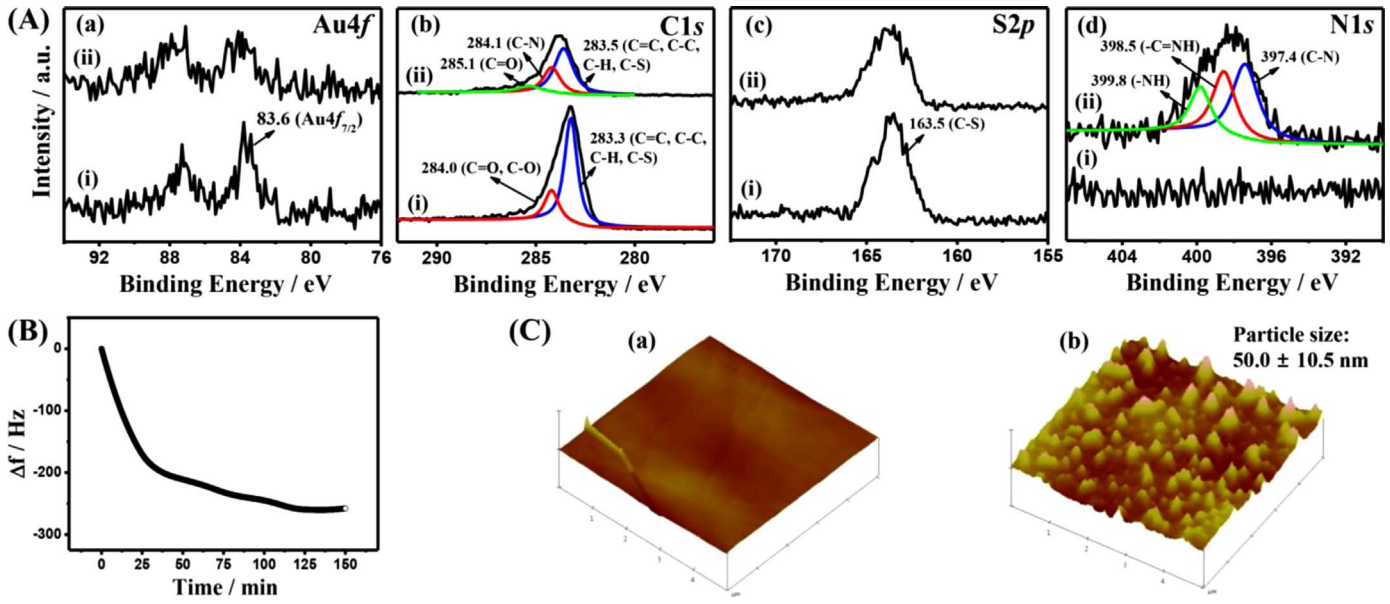


**Fig. 1.** (A) XPS spectra of (a(i)) Au4f for GCE/AuNPs and (a(ii)) GCE/AuNPs/pTTBA surface, (b) C1s, (c) S2p, and (d) N1s for (i) GCE/AuNPs/pTTBA and (ii) GCE/AuNPs/pTTBA/CapAnti. (B) Frequency changes during immobilization of CapAnti onto the Au-coated/pTTBA chip. (C) Tapping mode AFM images of the bare HOPG (left) and HOPG/nCOL (right) surfaces; images size is 500.0 nm × 500.0 nm.

shows an S2p peak at 163.5 eV corresponding to the C–S bond, which is due to the sulfur component of pTTBA (Fig. 1(A(c(i)))), however, it was not observed for GCE/AuNPs surface. The result clearly indicates the successful preparation of AuNPs-pTTBA composite. Furthermore, when we examined the deconvoluted N1s spectrum, clear peaks at 397.4, 398.5, and 399.8 eV was observed which corresponds to the C–N, –C=NH, and –NH bonds formation due to the covalent bond formation between $–NH_2$ groups of CapAnti and –COOH groups of pTTBA indicating successful CapAnti immobilization (Fig. 1(A(d(ii)))). No peak in N1s spectrum was observed for GCE/AuNPs/pTTBA surface indicating that these peaks were merely due to the CapAnti immobilization. In the next step, we investigated the real time immobilization of CapAnti using QCM based on the frequency change (Fig. 1(B)). For CapAnti immobilization, a decrease in the frequency reaches a complete steady state after about 130.0 ± 11 min with an overall frequency change ($\Delta f$) of 260 ± 17 Hz, corresponding to a mass change ($\Delta m$) of 285.7 ± 16.7 ng based on a previously defined equation (Noh et al., 2012). These results reconfirm the successfully immobilization of CapAnti onto the pTTBA layer. We also observed the surface of the sensor probe using SEM (figure not shown). The SEM image of the GCE/AuNPs layer shows the presence of the AuNPs with the particle sizes of 20.0 ± 1.5 nm whereas the GCE/AuNPs/pTTBA displays a thin film of pTTBA over the electrodeposited AuNPs. The TEM image of the electrodeposited AuNPs shows the size of 20.0 ± 1.5 nm, which is comparable to our previously reported result (Chandra et al., 2015).

We separately characterized the freshly prepared nCol by atomic force microscope in order to assess its size and morphology using highly oriented pyrolytic graphite (HOPG) electrode (Fig. 1(C)). The (a) HOPG and (b) HOPG/nCOL samples were prepared and analyzed by AFM in tapping mode (Fig. 1(C)). The HOPG/nCOL exhibits a homogeneous composition of small particles indicating the successful preparation of nCOL, however, the bare HOPG surface doesn't show any such particle on its surface. The particle size of HOPG/nCOL was determined to be 50.0 ± 10.5 nm. These size of the nCOL prepared in our case was comparable with a previously reported result (Nicklas et al., 2009).

### 3.2. FACS analysis and biocompatibility assay

The Ep-MCCs were subjected for FACS analysis prior to biosensing experiment to know its stage which is very important parameter for early stage detection of cancer cells (Chandra et al., 2011c). The DNA distribution data was obtained by analysis of propidium iodide binding which shows that the cell fraction contains the highest percentage of G1 phase (76.58%) and the other distribution of cell phase is 1.39% and 20.19% for S, and G2/M phases, respectively (Fig. 2). This clearly infers the Ep-MCCs under investigation are in the early stage of the cell cycle and has been detected using the fabricated nanobiosensor. The biocompatibility of the prepared conjugate was analyzed by MTT assay (inset Fig. 2) where the % viability for tested cells was 85 ± 3% ($n=3$) indicating that the prepared conjugate is biocompatable and has no toxic effect, therefore it can be applied for cytosensing. We also examined cytotoxicity of Hyd-MWCNT-AuNPs under the similar experimental conditions, where the % viability of cells was 59 ± 4%. The decrease % viability in the latter case was possibly due to the toxic effect of MWCNT which induces cellular cytotoxicity (Magrez et al., 2006; Patlolla et al., 2010). The (+) and (−) controls showed % viability of 94 ± 4 and 23 ± 1%, respectively, indicating the cells under investigation behaved differently to unlike conditions.

### 3.3. Detection of Ep-MCCs with the sensor probe

To ensure the interaction of sensor probe with Ep-MCCs, we firstly applied EIS to detect these cells. Enumerated Ep-MCCs (SK-BR3 cells) were incubated with GCE/AuNPs/pTTBA/CapAnti probe for 25 min to form GCE/AuNPs/pTTBA/CapAnti/Ep-MCC. After washing, the EIS spectra in the Nyquist plots were recorded in PBS where a sharp increase in the Rct value ($\Delta$Rct = 1100.15 ± 98.3 Ω) was observed after the interaction between $1 \times 10^3$ Ep-MCCs/mL and the probe, which shows that the prepared biosensor is able to detect Ep-MCCs (left inset Fig. 3(A)). In order to confirm the efficiency of Ep-MCCs detection using the biosensor, we treated the GCE/AuNPs/pTTBA/CapAnti probe with increasing number of Ep-MCCs, where the Rct value increased linearly between $1 \times 10^3$ and $1 \times 10^4$ Ep-MCCs/mL. A linear plot was obtained the having the regression equation as follows: $\Delta R_{ct}$ (Ω) = 1059.82 (± 126.95)+

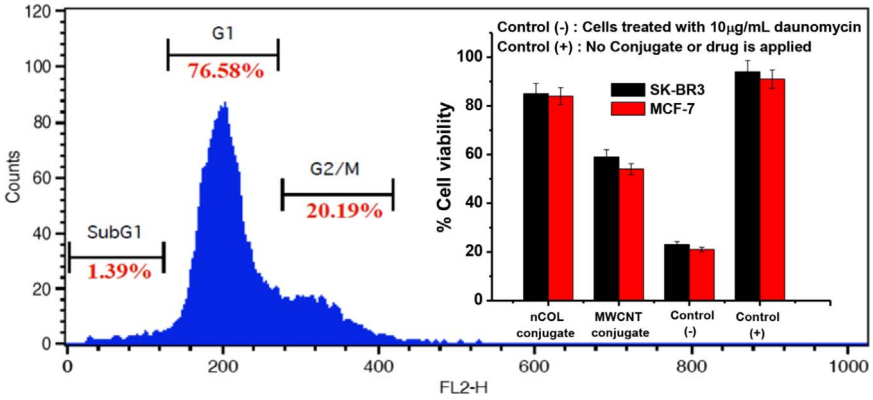


**Fig. 2.** FACS analysis showing distribution of Ep-MCC in each phase of cell cycle. Inset: biocompatibility evaluation of bioconjugates on SK-BR3 and MCF-7 cell line using MTT assay, control (−) and (+) represents the control experiment using anticancer drug and DMSO, respectively. Error bar shows the mean ± SD of three individual observations.

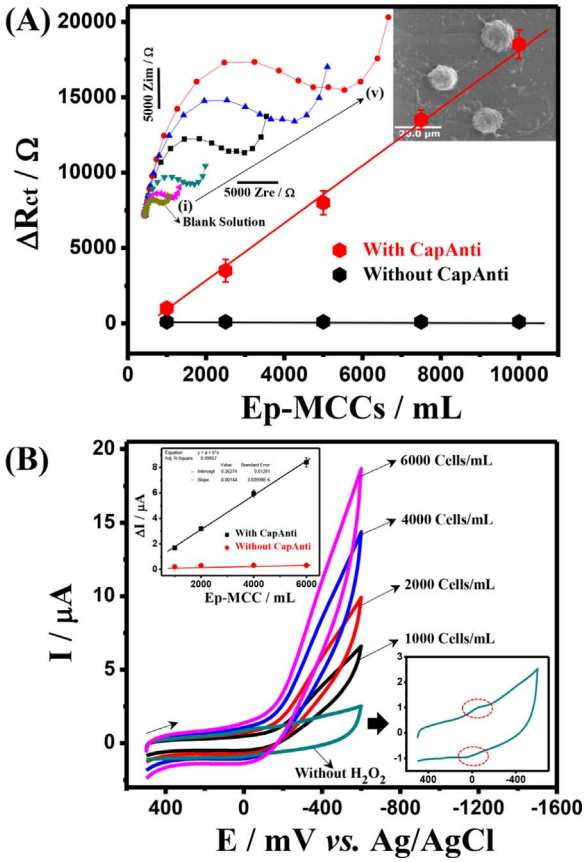


**Fig. 3.** (A) Linear plot for increasing number of Ep-MCC/mL interacted with GCE/AuNPs/pTTBA/CapAnti and GCE/AuNPs/pTTBA. Inset left: the obtained EIS signals recorded after Ep-MCC interaction in a 0.1 M PBS (pH 7.4) and Inset right: shows the SEM image of Ep-MCC captured by sensor probe. (B) CV response at GCE/AuNPs/pTTBA/CapAnti/Ep-MCC/RepAnti-nCOL-AuNPs-Hyd (green curve, separately shown as enlarge curve) in PBS at the scan rate of 50.0 mV $s^{-1}$. CVs recorded at GCE/AuNPs/pTTBA/CapAnti/Ep-MCC/RepAnti-nCOL-AuNPs-Hyd sensor with increasing number of Ep-MCC/mL in deoxygenated 0.1 M PBS containing 4.0 mM $H_2O_2$ (pH 7.4) at the scan rate of 50.0 mV $s^{-1}$. Inset shows the calibration plot for increasing number of Ep-MCC /mL. (For interpretation of the references to color in this figure legend, the reader is referred to the web version of this article.)

1.92 (± 0.047) [Ep-MCCs], with the correlation coefficient of 0.996 (Fig. 3(A)) ($n$=5). The interaction of Ep-MCCs with GCE/AuNPs/pTTBA (without CapAnti) was also tested, where no increase in the Rct was observed, indicating that the cellular aggregating at the biosensor surface was merely due to binding of Ep-MCCs with CapAnti (figure not shown). To confirm the binding of Ep-MCCs with the sensor probe surface, SEM images were collected. The inset (right) of Fig. 3(A) shows the presence of Ep-MCCs, indicating its successful capturing by the GCE/AuNPs/pTTBA/CapAnti probe.

Next, we detected Ep-MCCs using sandwich approach, where GCE/AuNPs/pTTBA/CapAnti/Ep-MCC probe was reacted with the RepAnti-nCOL-AuNPs-Hyd conjugate for 30 min. After binding and subsequent washing, the final GCE/AuNPs/pTTBA/CapAnti/Ep-MCC/RepAnti-nCOL-AuNPs-Hyd probe was subjected to three electrode electrochemical setup in a deoxygenated PBS. Then, cyclic voltammetry (CV) was performed by cycling the potential between +0.6 and −0.7 V at a scan rate of 50.0 mV $s^{-1}$. A redox peak at −50/−70 mV was observed due to the electrochemical behavior of Hyd itself (Fig. 3(B): green curve), which was directly proportional to the scan rate due to the surface-confined electrochemical reaction, indicating the successful interaction between RepAnti-nCOL-AuNPs-Hyd and GCE/AuNPs/pTTBA/CapAnti/Ep-MCC. In a control experiment, when nCOL-AuNP-Hyd (without RepAnti) was reacted with the GCE/AuNPs/pTTBA/CapAnti/Ep-MCC probe, no redox peak was observed, confirming that the Hyd redox peak appeared in the earlier case was merely due the immunreaction between captured Ep-MCCs and RepAnti attached conjugate. The ability of GCE/AuNPs/pTTBA/CapAnti/Ep-MCC/RepAnti-nCOL-AuNPs-Hyd probe to catalyze the reduction of $H_2O_2$ was further examined by recording CV in a deoxygenated PBS containing 4.0 mM $H_2O_2$. A distinct reduction peak at −400 mV was observed due to the reduction of $H_2O_2$ by Hyd attached on the sensor probe. The peak current at −400 mV increased with higher Ep-MCCs from 1000 to 6000 cells/mL (Fig. 3(B)) ($n$=5), however, no increase in the signal was observed when CapAnti was not immobilized. A linear plot is obtained (inset) with a linear regression equation expressed as follows: ΔI (μA)=0.262 (± 0.012)+0.0014 (± 0.0000038) [Ep-MCC], and has a correlation coefficient of 0.998 (inset Fig. 3(B)). Results based on EIS and CV clearly indicate that the developed nanobiosensor can accurately detect Ep-MCCs in a dose dependent manner in sandwich format.

### 3.4. Analytical performance of the sensor probe

At first, we optimized the experimental parameters of the sensor probe to obtain the best analytical performance for Ep-MCCs detection (Fig. 4). The optimized conditions are as follows; antibody concentration 50 μg/mL, temperature 35 °C, pH 7.5, and incubation time 25 min (details of optimization experiments are described in Supplementary material). Under the optimized conditions, the performance of the developed biosensor for quantitative detection of Ep-MCCs was performed using chronoamperometry. The inset of Fig. 5(A) displays the chronoamperometric responses of the developed biosensor at −0.45 V *vs.* Ag/AgCl (optimized) in deoxygenated PBS containing 4.0 mM $H_2O_2$ in

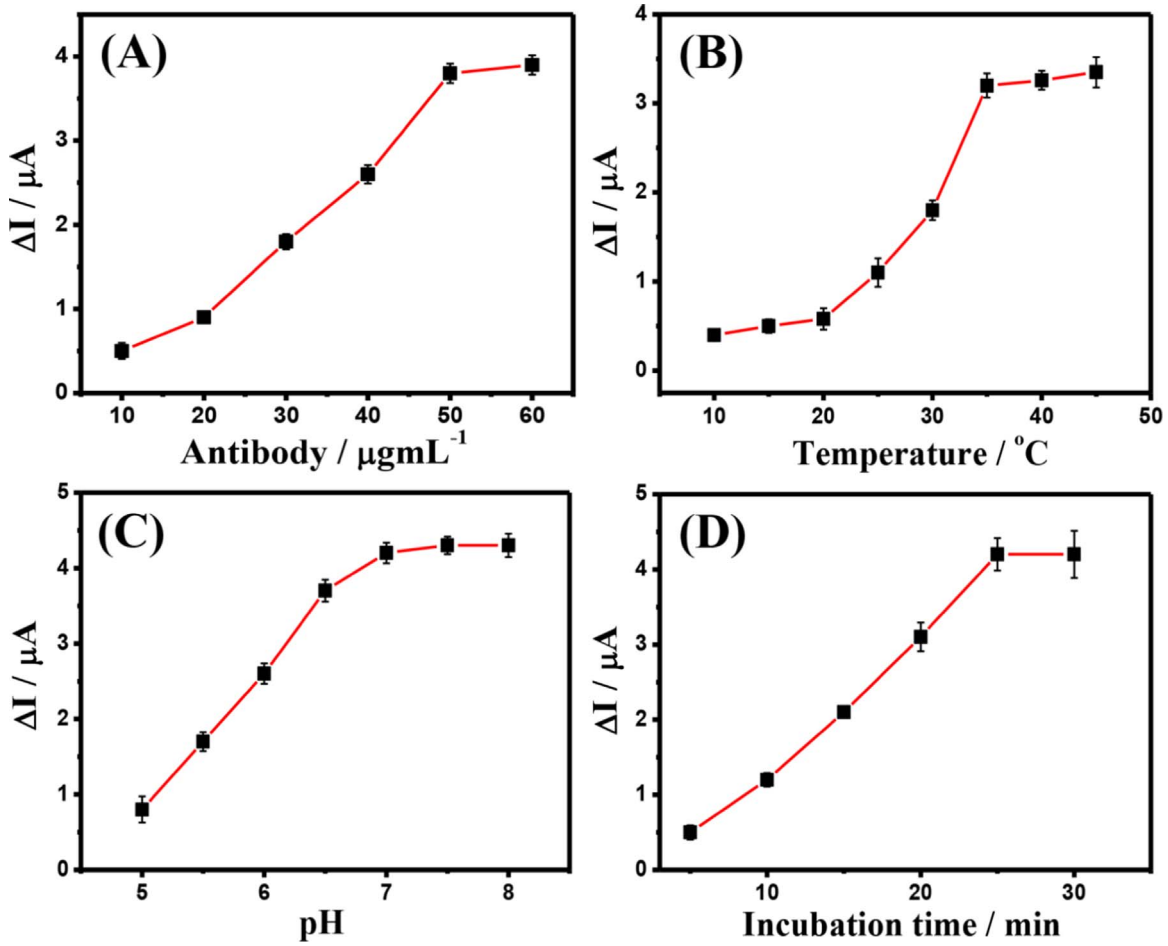


**Fig. 4.** Optimization of the experimental parameters: effects of (A) antibody concentration, (B) temperature, (C) pH, and (D) incubation time on analytical performance of sensor probe. The values on the y-axis shown in the histograms are based on the amperometric signals.

the absence and presence of different concentrations of Ep-MCCs. Chronoamperometry clearly shows increase in the current response with increase in the Ep-MCCs, indicating that the target cells are effectively detected by the developed sensor. Based on the data, a calibration plot was obtained, which showed a linear response for Ep-MCCs detection ranging from 45 to 100,000 Ep-MCCs/mL (Fig. 5(A)). The linear regression equation is expressed as follows: $\Delta I\ (\mu A) = 0.7039\ (\pm 0.0905) + 0.004363\ (\pm 0.0000024)$ [Ep-MCC] with the correlation coefficient of 0.981. The detection limit of Ep-MCCs was determined to be $28 \pm 3$ Ep-MCCs/mL (RSD < 5.4%) based on the standard deviation of five repeated measurements of the blank (95% confidence level, $n=5$). The obtained detection limit was significantly lower compared to earlier reported biosensors for Ep-MCCs detection (Arya et al., 2013; Kumeria et al., 2012). We also performed the similar experiment with another Ep-MCC type (*i.e.* MCF-7), where the response current increased with increase in the cell numbers, however, the detection limit for MCF-7 cells was $35 \pm 4$ cells/mL (RSD < 4.7%). A comparatively higher detection limit in the latter case was possibly due to the low concentration of the Ep-CAM on the cell membrane of MCF-7 cells.

### 3.5. Selectivity, reproducibility, stability, and real sample analysis

Selectivity assay was performed using HeLa, HEK-293, and jurkat cells at 1000, 30,000, and 100,000 cells/mL concentrations. Fig. 5(B) shows a comparative current response at different cells concentrations, where the negligible signal is observed for HeLa, HEK-293, and jurkat cells compared to target cells. This was possibly due to the absence of EpCAMs on the cell surface of the non-target cells, thereby no immunoreaction leading to no current response. We also tested the ability of the developed biosensor to detect target cells in a mixed cells sample by detecting them in presence of HeLa, HEK-293, and jurkat cells. Interestingly, the sensitivity of the detection in this case was 94.6% ($n=5$) compared when Ep-MCCs were detected alone, indicating the ability of selective detection of Ep-MCCs in a mixed cells population. We also performed series of control experiments to confirm the selectivity of the developed biosensor through testing the compounds that are majorly present in the real sample matrix such as; red blood cells, albumin, fibrinogens, and immunoglobulin G. No current response was observed for all the tested compounds which clearly indicate that the proposed biosensor is highly selective towards Ep-MCC detection. The reproducibility of the biosensor was evaluated which showed the RSD < 4.7 and electrode-to-electrode RSD was < 5.2% even when the same fabrication process was followed% ($n=5$). This minor variation was most likely due to the slight variation in the sensor fabrication process. Long term stability of the developed biosensor was assessed with respect to time, where it retained 94% of its sensitivity upto 5 weeks. The response decreased about 13% after five weeks and then gradually decreased with time. Thus, the sensor was reasonably stable up to five weeks.

The real biomedical application of the nanobiosensor was investigated by detecting Ep-MCCs in a human serum samples in the similar dynamic range (45–100,000 Ep-MCCs/mL) as done in the buffer solution. Serum has been extensively used as a model real sample matrix to demonstrate the cytosensing ability of

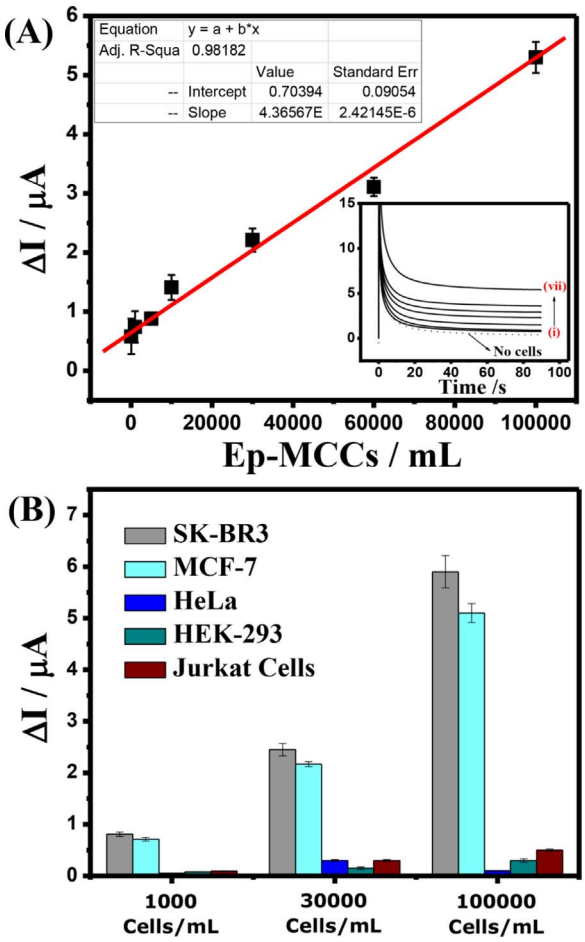


**Fig. 5.** (A) Calibration plot based on the signal obtained the amperometric responses for Ep-MCC detection using the biosensor with increasing number of Ep-MCC/mL [45–100,000 Ep-MCC/mL], all experiments were performed in deoxygenated PBS containing 4.0 mM $H_2O_2$ (pH 7.4), applied potential: −0.45 V *vs.* Ag/AgCl. (B) Histogram showing the selective detection of Ep-MCC using biosensor at 1000, 30,000, and 100,000 Ep-MCC/mL concentrations. The values on the y-axis shown in the histograms are based on the amperometric signals.

biosensors (Chandra et al., 2013; Moscovici et al., 2013). Thus, we detected Ep-MCCs in a serum sample where the current response was directly proportional to Ep-MCCs, indicating that the biosensor can effectively detect Ep-MCCs in a real sample matrix, hence valuable for direct clinical applications. The linear regression equation for the calibration plot in the serum sample is expressed as follows: $\Delta I\ (\mu A) = 0.6504\ (\pm 0.0832) + 3.851\ (\pm 0.0000036)$ [Ep-MCC] with the correlation coefficient of 0.978. The detection limit of Ep-MCC (SK-BR3) in a serum sample was determined to be $36 \pm 3$ cells/mL (RSD < 3.9%) based on the standard deviation of five repeated measurements of the blank (95% confidence level, $n=5$).

## 4. Conclusions

A selective biocompatable amperometric nanobiosensor has been designed and applied for the detection of metastatic cancer cells in biological fluids. The selective and sensitive detection of Ep-MCCs is achieved due to stable immobilization of monoclonal antibody and the application of electrocatalytic bioconjugate in the detection procedure. The developed nanobiosensor is able to detect the Ep-MCCs in mixed cells sample and in the presence of other chemical molecules present in the biological matrix. The stage of the target cells was analyzed by FACS, confirming that the detected cells were in early stage of cell cycle, which confirm the early detection of metastatic cancer cells using the proposed biosensor. A linear relationship for Ep-MCCs detection is observed over a range of 45–100,000 cells/mL with the detection limit of $28 \pm 3$ Ep-MCCs/mL. The developed sensor effectively detect Ep-MCCs in the biological fluids, therefore it can be further applied to detect these cells in clinical samples obtained from cancer patients. In future, the fabricated nanobiosensor prototype can be translated into a miniaturized commercial kit based diagnostic method for the point-of-care medical applications.

## Acknowledgements

This work was supported by the National Research Foundation of Korea (NRF) grant funded by the Korea government (MSIP) (No. 2015R1A2A1A13027762). Pranjal Chandra acknowledge DST Ramanujan Fellowship and Indian Institute of Technology-Guwahati startup grant BSBE/SG/IITG/PC1126/0001 for completion of this work.

## Appendix A. Supplementary material

Supplementary data associated with this article can be found in the online version at http://dx.doi.org/10.1016/j.bios.2016.05.092.

## References

Anderson, J.C., Eriksson, C., 1968. Nature 218, 166–168.
Arya, S.K., Wang, K.Y., Wong, C.C., Rahman, A.R., 2013. Biosens. Bioelectron. 41, 46–51.
Camacho, J., 2012. Molecular Oncology Principles and Recent Advances. Bentham Science Publishers, Maryland.
Chambers, A.F., Groom, A.C., MacDonald, I.C., 2002. Nat. Rev. Cancer 2, 563–572.
Chandra, P., Noh, H.-B., Won, M.-S., Shim, Y.-B., 2011a. Biosens. Bioelectron. 26, 4442–4449.
Chandra, P., Zaidi, S.A., Noh, H.-B., Shim, Y.-B., 2011b. Biosens. Bioelectron. 28, 326–332.
Chandra, S., Barola, N., Bahadur, D., 2011c. Chem. Commun. 47, 11258–11260.
Chandra, P., Koh, W.C.A., Noh, H.-B., Shim, Y.-B., 2012. Biosens. Bioelectron. 32, 278–282.
Chandra, P., Noh, H.-B., Shim, Y.-B., 2013. Chem. Commun. 7, 1900–1902.
Chandra, P., Noh, H.-B., Pallela, R., Shim, Y.-B., 2015. Biosens. Bioelectron. 70, 418–425.
de la Escosura, M., A., Sánchez, E.C., Díaz, F.B., González, F.A., Maltez-da Costa, M., Merkoçi, A., 2009. Anal. Chem. 81, 10268–10274.
Feng, L., Liu, Z., 2011. Nanomedicine 6, 317–324.
Hermanson, G.T., 2013. Bioconjugate Techniques, Third edition. Elsevier.
Karachaliou, N., Mayo-de-Las-Casas, C., Molina-Vila, M.A., Rosell, R., 2015. Ann. Transl. Med. 3, 36.
Katz, R.L., Weigong, H., Abha, K., Ricardo, L.F., Tanweer, M.Z., Matthew, K., Nancy, P. C., Hua-Zhong, Z., Feng, J., Margaret, R.S., David, P.B., Carlos, A.J., Reza, J.M., Stephen, G.S., Jack, R., Jeffrey, S.M., Carol, E., Randa, E., 2010. Clin. Cancer Res. 16, 3976–3987.
Koh, W.C.A., Chandra, P., Kim, D.-M., Shim, Y.-B., 2011. Anal. Chem. 83, 6177–6183.
Königsberg, R., Obermayr, E., Bises, G., Pfeiler, G., Gneist, M., Wrba, F., de Santis, M., Zeillinger, R., Hudec, M., Dittrich, C., 2011. Acta Oncol. 50, 700–710.
Krebs, M.G., Hou, J.-M., Ward, T.H., Blackhall, F.H., 2010. Ther. Adv. Med. Oncol. 2, 351–365.
Kumeria, T., Kurkuri, M.D., Diener, K.R., Parkinson, L., Losic, D., 2012. Biosens. Bioelectron. 35, 167–173.
Magrez, A., Kasas, S., Salicio, V., Pasquier, N., Seo, J.W., Celio, M., Catsicas, S., Schwaller, B., Forró, L., 2006. Nano Lett. 6, 1121–1125.
Moscovici, M., Bhimji, A., Kelley, S.-O., 2013. Lab Chip 13, 940–946.
Mukherjee, S., Venugopal, J.R., Ravichandran, R., Ramakrishna, S., Raghunath, M., 2011. Adv. Funct. Mater. 21, 2291–2300.
Nagrath, S., Sequist, lV., Maheswaran, S., Bell, D.W., Irimia, D., Ulkus, L., Smith, M.R., Kwak, E.L., Digumarthy, S., Muzikansky, A., Ryan, P., Balis, U.J., Tompkins, R.G., Haber, D.A., Toner, M., 2007. Nature 450, 1235–1239.
Nicklas, M., Schatton, W., Heinemann, S., Hanke, T., Kreuter, J., 2009. Drug Dev. Ind. Pharm. 35, 1035–1042.
Noh, H.-B., Chandra, P., Moon, J.-O., Shim, Y.-B., 2012. Biomaterials 33, 2600–2607.
Panchapakesan, B., Caprara, R., Velasco, V., Loomis, J., King, B., Xu, P., Burkhead, T., Sethu, P., Stallons, L.J., McGregor, W.G., Rai, S.N., Kloecker, G., Wickstrom, E.,

2010. Cancer Nanotechnol. 1, 3–11.
Patlolla, A., Knighten, B., Tchounwou, P., Ethn, Dis, 2010. Winter 20 (S1), S65–S72.
Pecorino, L., 2012. Molecular Biology of Cancer: Mechanisms, Targets, and Therapeutics, third edition. Oxford University Press, Oxford.
Rahman, Md.A., Kumar, P., Park, D.-S., Shim, Y.-B., 2008. Sensors 8, 118–141.
Skirecki, T., Hoser, G., Kawiak, J., Dziedzic, D., Domagała-Kulawik, J., 2014. Arch. Immunol. Ther. Exp. 62, 67–75.
Spizzo, G., Fong, D., Wurm, M., Ensinger, C., Obrist, P., Hofer, C., Mazzoleni, G., Gastl, G., Went, P., 2011. J. Clin. Pathol. 64, 415–420.
Srivastava, A., Aggarwal, L., Jain, N., 2015. ACS Comb. Sci. 17, 39–48.
Zhang, Y., Ali, S.F., Dervishi, E., Xu, Y., Li, Z., Casciano, D., Biris, A.S., 2010. ACS Nano 4, 3181–3186.
Zhao, S., Yang, H., Zhang, M., Zhang, D., Liu, Y., Liu, Y., Song, Y., Zhang, X., Li, H., Ma, W., Zhang, Q., 2013. Cell Biochem. Biophys. 65, 263–273.
Zhu, Y., Chandra, P., Shim, Y.-B., 2013. Anal. Chem. 85, 1058–1064.
Zhu, Y., Son, J.I., Shim, Y.-B., 2010. Biosens. Bioelectron. 26, 1002–1008.